Robust SLAM System Based on Extended Risk-Sensitive Filter

Yuxiang Liang, Huihong Zhao, Xujie Li, Baoyu Wang, Peibo Li, and Yiyang Zhao*

Abstract— **Designing robust estimators under noise parameter uncertainty is a challenging task. Indeed, due to environmental variations, differences in measurement distances, and sensor degradation, the Gaussian assumption of measurement noise is overly optimistic at certain stages. Therefore, these overly optimistic assumptions may lead to inaccurate estimations. Building on the foundation of the Risk-Sensitive Filter (RSF) for linear systems, this paper present an Extended Risk-Sensitive Kalman Filter (ERKF) for nonlinear systems and applies it to backend pose estimation in the simultaneous localization and mapping (SLAM) problem. This method formulates state estimation as a suboptimal estimation problem of solving a risk-sensitive criterion, thereby enhancing the robustness of the estimator. Extensive experiments on both benchmark and private datasets demonstrated that the proposed system achieves enhanced robustness without compromising accuracy. We evaluated the performance of the ERKF algorithm in simulation experiments for unmanned helicopter state estimation under conditions of noise uncertainty. The simulation results demonstrated significant improvements over the traditional EKF-SLAM algorithm. Multiple sequences from a publicly available radar dataset were tested and compared. The results indicate that the accuracy of the FAST-LIO2 and Point-LIO frameworks based on ERKF is comparable to, or even marginally superior to, that of the original algorithms. It is worth noting that most of these datasets were collected in relatively stable noise environments, where the point cloud noise parameters typically adhere to the given white noise assumption. To further validate the algorithm's robustness, we conducted challenging real-world experiments in specialized environments with metallic walls and narrow metallic pipeline. In these scenarios, the SLAM system based on ERKF demonstrated higher state estimation accuracy.**

I. Introduction

SLAM is a task worthy of attention, and it has wide applications in many fields, such as navigation for autonomous vehicles, autonomous positioning of UAV and augmented reality [1-6]. SLAM algorithms enable a robot or autonomous system to build a map of an unknown environment while simultaneously keeping track of its own location within that environment. In practical applications, the performance and robustness of the SLAM system will directly affect the practicality and reliability of the robot.

With the continuous development of technology, the SLAM problem has been widely studied and a variety of solutions have emerged. Among them, optimization-based and filter-based are two common paradigms for solving SLAM problems. Optimization-based SLAM techniques [7-9], such as Graph SLAM, leverage optimization algorithms to refine the robot's pose estimation and map representation iteratively. These methods excel in providing globally consistent solutions but usually require high computational complexity and memory requirements, are sensitive to initial values and converge slowly, which limits their performance in real-time and robustness. The following frameworks have been optimized in different aspects. Ground-Fusion is a low-cost SLAM system that tightly integrates RGB-D, IMU, wheel odometry, and GNSS signals, featuring robust initialization, sensor anomaly detection, and real-time dense mapping for reliable localization in diverse environments [7]. MAVIS is an optimization-based visual-inertial SLAM system designed for multi-camera setups, incorporating an improved IMU pre-integration formulation based on the $SE_2(3)$ exponential, which enhances tracking performance under fast rotations and extended integration times [8]. LIO-SAM is a tightly-coupled lidar-inertial odometry framework based on smoothing and mapping. It leverages factor graph optimization to fuse multi-sensor data and enhances real-time performance through a local sliding window matching strategy [9].

In comparison, filter-based SLAM methods have high potential and feasibility in practical applications due to their simplicity and efficiency. The Extended Kalman Filter (EKF) and its variants are widely used in SLAM frameworks. M. Li and A. Mourikis proposed a novel multi-state constrained Kalman filter (MSCKF), which has higher accuracy and consistency than the iterative sliding window fixed-delayed smoother [10]. Through simulation experiments, Y. Zhang and T. Zhang et al. showed that in most scenarios with actual noise levels, the accuracy of SLAM algorithm based on EKF is very close to that of SLAM algorithm based on nonlinear optimization [11]. A. Barrau and S. Bonnabel analyzed the convergence properties of the Invariant Extended Kalman Filter (IEKF) as a nonlinear observer on Lie groups and proved its local stability [12]. P. Wu and Z. Shi et al. proposed an improved EKF-SLAM algorithm for the autonomous landing of unmanned helicopters [13]. FAST-LIO2 is a direct and robust LiDAR-inertial odometry framework that eliminates the feature extraction module and employs an efficient incremental k-d tree (ikd-Tree) for real-time mapping. Meanwhile, FAST-LIO2 optimizes the computation of the Kalman gain to reduce the computational cost of matrix inversion, significantly improving speed and accuracy across various environments [14]. Point-LIO proposes a robust, high-bandwidth LiDAR-inertial odometry framework that leverages point-by-point state updates and a stochastic process-augmented kinematic model to achieve high-

*Resrach supported by Open Research Fund Program of Data Recovery Key Laboratory of Sichuan Province (Grant No. DRN2307).

Y. Liang was with school of Mathematics and Statistics, Qilu University of Technology (Shandong Academy of Science), Jinan, 250353, China;

H. Zhao is with school of Mathematics and Statistics, Qilu University of Technology (Shandong Academy of Sciences), Jinan 250353, China;

X. Li was with the Shanghai Juanji Special Equipment Co., Ltd.;

B. Wang is with the Shanghai Juanji Special Equipment Co., Ltd.;

P. Li, is with school of Mechanical Engineering, Donghua University, Shanghai, 201620, China;

Y. Zhao, is with school of Mechanical Engineering, Shanghai Jiao Tong University, Shanghai, 200240, China.

frequency odometry and accurate mapping under aggressive motions and IMU saturation [15]. FAST-LIVO2 proposes an innovative direct LiDAR-inertial-visual odometry framework, addressing the dimension mismatch between LiDAR and visual measurements through the introduction of a sequential update strategy in the ISEKF. Additionally, the system significantly improves image alignment accuracy and robustness by utilizing plane priors from LiDAR points [16]. These methods model the SLAM problem as a state estimation problem and use recursive Bayesian filters to estimate and update the robot's state. They can process the noise of sensor data and the dynamic changes of the environment in real time, thereby improving the robustness and stability of the system.

Despite their computational advantages, traditional filter-based SLAM methods have certain limitations. These factors include sensitivity to nonlinearity, especially in environments with significant uncertainty or when faced with sudden changes. Furthermore, their reliance on Gaussian assumptions often leads to obtaining an incorrect optimal solution, particularly in scenarios where noise follows a non-Gaussian distribution. To address the limitations of traditional filtering techniques, B. Hassibi and A. Sayed et al. introduced the RSF as a robust state estimation method. By incorporating risk-sensitive criteria into the estimator, RSF enhances the ability to handle noise uncertainty more effectively [17, 18]. A. Jordana and A. Meduri et al. employed the Gauss-Newton method to solve the max-min optimization problem derived from dynamic game control theory, effectively addressing estimation uncertainty and improving the robustness of Model Predictive Control (MPC) [19]. Y. Luo and Q. Su et al. proposed an improved Rao-Blackwellized particle filtering algorithm, which can avoid the calculation of Jacobian matrix and the accumulation of linearization errors [20]. OpenVINS introduces an on-manifold sliding window Kalman filter framework and incorporates a consistent First-Estimates Jacobian (FEJ) treatment for SLAM landmarks, enhancing estimation accuracy and stability [21].

To the best of the author's knowledge, the application of ERKF in SLAM problems has not yet been reported. Therefore, based on the theory of RSF for linear systems, we discuss the pose estimation of the SLAM problem in a general state-space model. In this problem, our objective is to minimize a risk-sensitive performance index. Based on the EKF theory, the state-space model of the nonlinear system in the Grein space is linearized, and a detailed derivation of the recursive process of the nonlinear system's ERKF is provided. The main contributions of this paper are as follows: (i) To the best of our knowledge, this is the first work to propose a SLAM algorithm based on the ERKF, expanding the application of filtering techniques in SLAM. (ii) The proposed ERKF is capable of handling both known and unknown noise parameters, providing enhanced robustness and offering a theoretical foundation for applying SLAM in complex environments. Extensive experiments were conducted to evaluate the performance of the proposed algorithm, demonstrating its effectiveness under conditions of noise parameter uncertainty. (iii) The max-min problem of the complex RSF in nonlinear systems is transformed into a KF problem through Krein state-space projection. The resulting solution is recursive, ensuring the real-time performance of the system.

The remainder of this paper is organized as follows. Section II introduces the system description and the recursive process of the EKF. Section III presents the design methodology of the ERKF under two risk-sensitive parameter settings and introduces the general framework of the ERKF-SLAM algorithm. Section IV validates the effectiveness of the ERKF algorithm through simulations, open-source datasets, and real-world experiments. Finally, we conclude the paper with a summary of the findings.

II. MATERIALS AND METHODS

Consider the nonlinear discrete system described by

$$x_{k+1} = f(x_k, u_k) + w_k, \tag{1}$$

$$y_k = h(x_k) + v_k, \tag{2}$$

where $f(\cdot)$ and $h(\cdot)$ are nonlinear functions, k is the discrete time, $x_k \in R^n$ is the unknown system state, $u_k \in R$ is the system input, $y_k \in R^m$ is the system measurement, process noise $w_k \in R^n$ and measurements noise $v_k \in R^m$ are white noise of the system.

A. Extended Kalman Filter

To design the ERKF for nonlinear systems, we introduce the EKF recursive process for discrete-time nonlinear systems. The discrete-time approach is adopted because, even if the fundamental state process is continuous, performing integration in the continuous-time EKF imposes a significant computational burden on the computer. Therefore, the dynamic system is typically discretized, and state estimation is then achieved through the EKF. The recursive process of the EKF is as follows:

$$\hat{x}_{k+1}^- = f(\hat{x}_k^+, u_k),$$

$$\hat{y}_{k+1}^- = h(\hat{x}_{k+1}^-),$$

$$\varepsilon_{k+1} = y_{k+1} - \hat{y}_{k+1}^-,$$

$$P_{k+1}^- = F_k P_k^+ F_k^{\mathrm{T}} + Q,$$

$$K_{k+1} = P_{k+1}^- H_{k+1}^{\mathrm{T}} (H_{k+1} P_{k+1}^- H_{k+1}^{\mathrm{T}} + R)^{-1},$$

$$\hat{x}_{k+1}^+ = \hat{x}_{k+1}^- + K_{k+1}\varepsilon_{k+1},$$

$$P_{k+1}^+ = (I - K_{k+1}H_{k+1})P_{k+1}^-.$$

Remark 1. *It is worth noting that the KF gives an unbiased optimal estimate for a linear system, while the EKF gives an optimal posterior estimate under a first-order linear approximation of the nonlinear problem posed by SLAM.*

III. NUMERICAL ANALYSIS RESULTS

A. Design of risk-sensitive estimator for nonlinear systems

Consider the Hilbert state-space model (1) and (2), construct the risk-sensitive performance index as follows:

$$\mu_k(\theta) = -\frac{2}{\theta} log\left[Eexp\left(-\frac{\theta}{2}C_k\right)\right], \tag{3}$$

$$C_k = \sum_{i=0}^{k} \left(\check{z}_{i|l} - Lx_i\right)^{\mathrm{T}} \left(\check{z}_{i|l} - Lx_i\right). \quad (4)$$

where $\check{z}_{i|l}$ is defined as the estimate of the measurement value z_i, and we can easily see that $E(C_k)$ is the performance index of H^2 estimators.

The exponential cost criterion in (3) corresponds to the following minimization problem

$$\min_{\{\check{z}_{k|l}\}} \mu_k(\theta) = \min_{\{\check{z}_{k|l}\}} -\frac{2}{\theta} log\left[Eexp(-\frac{\theta}{2}C_k)\right], \quad (5)$$

where parameter θ is called the risk-sensitivity parameter, any filter that minimizes $\mu_k(\theta)$ is called RSF.

Further, it can be obtained from the joint conditional distribution formula as follows

$$E\left(\exp\left(-\frac{\theta}{2}C_k\right)\right) =$$

$$\int exp\left[-\frac{\theta}{2}C_k\right] p(x_0, w_0, \dots, w_k | y_0, \dots, y_k) dx_0 dw_0 \cdots dw_k$$

$$\propto \int exp\left[-\frac{\theta}{2}C_k\right] exp\left[-\frac{1}{2}J_k\right] dx_0 dw_0 \cdots dw_k, \quad (6)$$

$$J_k = x_0^{\mathrm{T}} \mathcal{P}_0^{-1} x_0 + \sum_{i=0}^{k} w_i^{\mathrm{T}} Q^{-1} w_i + \sum_{i=0}^{k} \varepsilon_i^{\mathrm{T}} R^{-1} \varepsilon_i, \quad (7)$$

which shows that the risk-sensitive criterion can be alternatively written as

$$\theta > 0: \max_{\{\check{z}_{k|l}\}} \int exp\left[-\frac{\theta}{2}C_k - \frac{1}{2}J_k\right] dx_0 dw_0 \cdots dw_k, \quad (8)$$

$$\theta < 0: \min_{\{\check{z}_{k|l}\}} \int exp\left[-\frac{\theta}{2}C_k - \frac{1}{2}J_k\right] dx_0 dw_0 \cdots dw_k, \quad (9)$$

This suggests that a new minimization performance index is defined:

$$\tilde{J}_k = J_k + \theta C_k$$

$$= x_0^{\mathrm{T}} \mathcal{P}_0^{-1} x_0 + \sum_{i=0}^{k} w_i^{\mathrm{T}} Q^{-1} w_i$$

$$+ \sum_{i=0}^{k} \varepsilon_i^{\mathrm{T}} R^{-1} \varepsilon_i + \theta \sum_{i=0}^{k} \left(\check{z}_{k|l} - Lx_i\right)^{\mathrm{T}} \left(\check{z}_{k|l} - Lx_i\right). \quad (10)$$

To deal with extreme values, we must to make sure that the integrals of (8) and (9) are finite.

Lemma 1 (Finiteness Condition lemma). *The integral*

$$\int exp\left[-\frac{1}{2}\tilde{J}_k\right] dx_0 dw_0 \cdots dw_k$$

is finite iff (if and only if) $\tilde{J}_i$ has a minimum over $\{x_0, w_0, \cdots, w_k\}$. In that case it is proportional to

$$exp\left[-\frac{1}{2}\min_{x_0,w} \tilde{J}_k\right].$$

The above lemma thus reduces the risk-sensitive problem to one of finding the minimum of a second-order scalar form. More precisely, the criterion becomes

$$\theta > 0: \max_{\{\check{z}_{k|l}\}} \left\{\min_{x_0,w} \tilde{J}_k\right\},$$

$$\theta < 0: \min_{\{\check{z}_{k|l}\}} \left\{\min_{x_0,w} \tilde{J}_k\right\}.$$

To solve the above problem, we can introduce the following auxiliary Krein state-space model that corresponds to the quadratic form $\tilde{J}_i$

$$\boldsymbol{x}_{k+1} = f(\boldsymbol{x}_k, \boldsymbol{u}_k) + \boldsymbol{w}_k, \quad (11)$$

$$\begin{bmatrix} \boldsymbol{y}_k \\ \check{\boldsymbol{z}}_{k|k} \end{bmatrix} = \begin{bmatrix} h(\boldsymbol{x}_k) \\ L_k \boldsymbol{x}_k \end{bmatrix} + \boldsymbol{v}_k, \quad (12)$$

where

$$\left\langle \begin{bmatrix} \boldsymbol{x}_0 \\ \boldsymbol{w}_i \\ \boldsymbol{v}_i \end{bmatrix}, \begin{bmatrix} \boldsymbol{x}_0 \\ \boldsymbol{w}_j \\ \boldsymbol{v}_j \end{bmatrix} \right\rangle = \begin{bmatrix} \mathcal{P}_0 & 0 & 0 \\ 0 & Q\delta_{ij} & 0 \\ 0 & 0 & \begin{bmatrix} R & 0 \\ 0 & \theta^{-1} I \end{bmatrix} \delta_{ij} \end{bmatrix}.$$

Given the system (11), (12). A posteriori ERKF for a given $\theta > 0$, the risk-sensitive estimation problem always has a solution. For a given $\theta < 0$, a solution exists iff

$$\begin{bmatrix} R & 0 \\ 0 & \theta^{-1} I \end{bmatrix} \text{ and } R_{e,k} = \begin{bmatrix} R & 0 \\ 0 & \theta^{-1} I \end{bmatrix} + \begin{bmatrix} H_k \\ L_k \end{bmatrix} P_k \begin{bmatrix} H_k^{\mathrm{T}} & L_k^{\mathrm{T}} \end{bmatrix}$$

have the same inertia for all $i = 0, 1, \cdots, n,$ where $P_0 = \mathcal{P}_0$ and

$$P_{k+1} = F_k P_k F_k^{\mathrm{T}} + Q - F_k P_k \begin{bmatrix} H_k^{\mathrm{T}} & L_k^{\mathrm{T}} \end{bmatrix} R_{e,k}^{-1} \begin{bmatrix} H_k \\ L_k \end{bmatrix} P_k F_k^{\mathrm{T}},$$

$$\varepsilon_k = \begin{bmatrix} y_k - h(\hat{x}_k^-) \\ \check{z}_{k|k} - \hat{z}_{k|k-1} \end{bmatrix}.$$

The one-step update process of the ERKF with parameter is given by

$$\check{z}_{k|k} = L_k \hat{x}_k^+,$$

$$\hat{x}_{k+1}^- = f(\hat{x}_k^+, u_k),$$

$$\hat{x}_{k+1}^+ = F_k \hat{x}_k^+ + K_{k+1}\left(y_{k+1} - h(\hat{x}_{k+1}^-)\right),$$

$$K_{k+1} = P_{k+1} H_{k+1}^{\mathrm{T}} (R + H_{k+1} P_{k+1} H_{k+1}^{\mathrm{T}})^{-1}.$$

The derivation process can be found in Appendix A.

Algorithm 1: ERKF

Initialization: $\hat{x}_0^+ = x_0, \hat{P}_0^+ = \mathcal{P}_0, Q, R;$

Predict:

$\hat{x}_{k+1}^- = f(\hat{x}_k^+, u_k);$

$\hat{P}_{k+1}^- = F_k \hat{P}_k^+ F_k^T + Q;$

Update:

$\hat{x}_{k+1}^+ = \hat{x}_{k+1}^- + K_{k+1}\big(y_{k+1} - h(\hat{x}_{k+1}^-)\big);$

$K_{k+1} = \hat{P}_{k+1}^- H_{k+1}^T (R + H_{k+1} P_{k+1} H_{k+1}^{\mathrm{T}})^{-1};$

$\hat{P}_{k+1}^+ = \left(I - \hat{P}_{k+1}^- [H_{k+1}^T \quad L_{k+1}^T] R_{e,k+1}^{-1} \begin{bmatrix} H_{k+1} \\ L_{k+1} \end{bmatrix}\right) \hat{P}_{k+1}^-.$

B. ERKF-SLAM

We introduce a risk-sensitive criterion into a type of EKF-SLAM system to enhance the robustness of the filter by mitigating the effects of instability in observation noise parameters. The state vector of this system describes the robot pose and N sets of environmental landmark points. By setting the value of θ, a state-space model is constructed in the Krein space. Based on actual measurement results, the robot's pose and the 3D coordinates of the landmark points are estimated, and the prediction matrix and covariance matrix are updated.

The system state vector is represented as follow:

$$X_k = \left[x_k^{\mathrm{T}}, m_{1,k}^{\mathrm{T}}, m_{2,k}^{\mathrm{T}}, \cdots, m_{N,k}^{\mathrm{T}}\right]^{\mathrm{T}}. \tag{13}$$

Assuming that the feature points are at rest, the parameter matrix of the position information of the feature points m_i is the identity matrix I_3, and its value is only affected by the measurement noise of the sensors.

The complete Krein state-space model is presented below:

$$\boldsymbol{X}_k = \begin{bmatrix} f(\boldsymbol{x}_k, \boldsymbol{u}_k) \\ \boldsymbol{m}_{1,k} \\ \boldsymbol{m}_{2,k} \\ \vdots \\ \boldsymbol{m}_{N,k} \end{bmatrix} + \begin{bmatrix} \boldsymbol{w}_k \\ 0 \\ 0 \\ \vdots \\ 0 \end{bmatrix}, \tag{14}$$

$$\begin{bmatrix} \boldsymbol{Y}_{k,i} \\ \check{z}_{k|k} \end{bmatrix} = \begin{bmatrix} h_i(\boldsymbol{x}_k) \\ L_k \boldsymbol{X}_k \end{bmatrix} + \boldsymbol{v}_k. \tag{15}$$

Linearization of the nonlinear terms to the first-order gives the linear system as follows:

$$\begin{bmatrix} \boldsymbol{x}_{k+1} \\ \boldsymbol{m}_{1,k+1} \\ \boldsymbol{m}_{2,k+1} \\ \vdots \\ \boldsymbol{m}_{N,k+1} \end{bmatrix} = \begin{bmatrix} F_k & 0 & 0 & \cdots & 0 \\ 0 & I_3 & 0 & \cdots & 0 \\ 0 & 0 & I_3 & \cdots & 0 \\ \vdots & \vdots & \vdots & \ddots & \vdots \\ 0 & 0 & 0 & \cdots & I_3 \end{bmatrix} \begin{bmatrix} \boldsymbol{x}_k \\ \boldsymbol{m}_{1,k} \\ \boldsymbol{m}_{2,k} \\ \vdots \\ \boldsymbol{m}_{N,k} \end{bmatrix}$$

$$+ \begin{bmatrix} \tilde{\boldsymbol{u}}_{k,1} + \boldsymbol{u}_k \\ 0 \\ 0 \\ \vdots \\ 0 \end{bmatrix} + \begin{bmatrix} \boldsymbol{w}_k \\ 0 \\ 0 \\ \vdots \\ 0 \end{bmatrix}, \tag{16}$$

$$\begin{bmatrix} \boldsymbol{Y}_{k,i} \\ \check{z}_{k|k-1} \end{bmatrix} = \begin{bmatrix} H_{i,k} \boldsymbol{X}_k + \tilde{\boldsymbol{u}}_{k,2} \\ L_k \boldsymbol{X}_k \end{bmatrix} + \boldsymbol{v}_k. \tag{17}$$

where $F_k = \frac{\partial f}{\partial(x,y,z,\theta,\varphi)}, H_{i,k} = \left[-H_k, 0, \cdots, H_{m_i}, \cdots, 0\right], H_k = \frac{\partial h_i}{\partial(x,y,z,\theta,\varphi)}, H_{m_i} = \frac{\partial h_i}{\partial(x_i,y_i,z_i)}$, u_k is the known control input, $\tilde{u}_{k,1}$ and $\tilde{u}_{k,2}$ are the inputs generated by the linearization of the system.

Given the system (14), (15), and Theorem 1. For any θ, if the condition of ERKF is satisfied, then the ERKF as follows:

$$\check{z}_{k|k} = L_k \hat{X}_k^+,$$

$$\hat{P}_{k+1}^- = F_k \hat{P}_k^+ F_k^{\mathrm{T}} + Q,$$

$$\hat{X}_{k+1}^- = \left[f(\hat{x}_k^+, u_k), m_{1,k}, \cdots, m_{N,k}\right]^{\mathrm{T}},$$

$$\hat{P}_{k+1}^+ = \left(I - \hat{P}_{k+1}^- \left[H_{i,k+1}^T \quad L_{k+1}^T\right] R_{e,k+1}^{-1} \begin{bmatrix} H_{i,k+1} \\ L_{k+1} \end{bmatrix}\right) \hat{P}_{k+1}^-,$$

$$K_{k+1} = \hat{P}_{k+1}^- H_{i,k+1}^{\mathrm{T}} (R + H_{i,k+1} \hat{P}_{k+1}^- H_{i,k+1}^{\mathrm{T}})^{-1},$$

$$\hat{X}_{k+1}^+ = \hat{X}_{k+1}^- + K_{k+1}\left(Y_{i,k} - h_i(\hat{x}_k^-)\right),$$

where $Q = diag(Q_w, 0, \cdots, 0), R = diag(R_v, \theta^{-1} I).$

IV. EXPERIMENTS

A. Numerical simulation

This section validates the effectiveness of the proposed algorithm through numerical simulations of the autonomous landing problem of an unmanned helicopter. The motion and measurement equations are referenced from [13]. These equations describe the position and orientation angles of the unmanned helicopter in the world coordinate system, while the measurement equations characterize the positional relationships between the feature points and the unmanned helicopter. It should be noted that during the measurement process, the sensor can only observe the feature points within a certain distance.

Establish the unmanned helicopter pose information vector as follows:

$$x_k = [x(k), y(k), z(k), \theta(k), \varphi(k)]^{\mathrm{T}},$$

where $(x(k), y(k), z(k))$ is the position of the unmanned helicopter in the world coordinate system, $\theta(k), \varphi(k)$ are the pitch and yaw angles, respectively.

The measurement $y_{i,k}$ consists of the distance $\gamma_i(k)$, pitch angle $\theta_i(k)$ and yaw angle $\varphi_i(k)$. It is obtained through sensors as follows:

$$y_{i,k} = [\gamma_i(k), \theta_i(k), \varphi_i(k)]^{\mathrm{T}}.$$

Consider the state system of an unmanned helicopter, as described in (14) and (15), where the process noise vector w_k and the measurement noise $\boldsymbol{v}_k$ are zero-mean Gaussian white noises with variances $Q = diag(0.1, 0.1, 0.1, 0, 0)$ and $R = diag(0.01, 0.01, 0.01, \theta^{-1} I_5)$, respectively.

In this numerical simulation, set initial value $\chi_0 = (0,0,200,0,0.1)$, $\mathcal{P}_0 = diag(0.1,0.1,0.1,0,0)$, $\theta = -0.004$

and the sampling period is $0.2s$. Set constant angular velocity $v = 3\ m/s$, constant angular velocity $\omega_\theta = 0.7\ rad/s$, $\omega_\varphi = 0.7\ rad/s$. It should be noted that the real value of R was set to $diag(0.4, 0.4, 0.4)$. The unmanned helicopter moves according to the trajectory set by the landmarks, estimates and corrects the pose by observing feature points, and then calculates the corresponding control quantity to realize navigation. Figure 2 shows the true trajectory of the unmanned helicopter and its ERKF estimation in a two-dimensional plane considering only x and y coordinates. Figure 3 shows the true trajectory of the unmanned helicopter moving along the landmark and the ERKF estimate of its pose. We conducted ten tests in this simulation environment, as shown in Table 1. It can be observed that ERKF has significant advantages over EKF, especially in terms of accuracy and robustness, providing more stable and lower RMSE in various environments. This advantage may stem from the design of ERKF, which can better handle the uncertainty of noise and provide more precise state estimation.

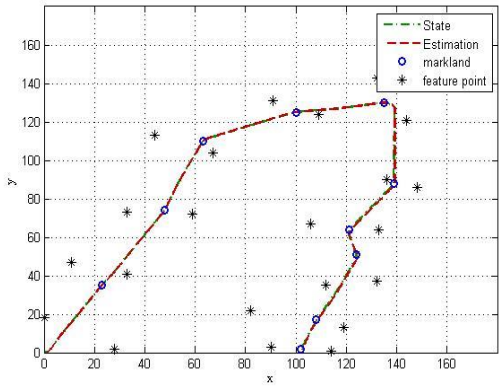

Figure 1. Two-dimensional plane true trajectory (green curve) and estimation of ERKF (red curve)

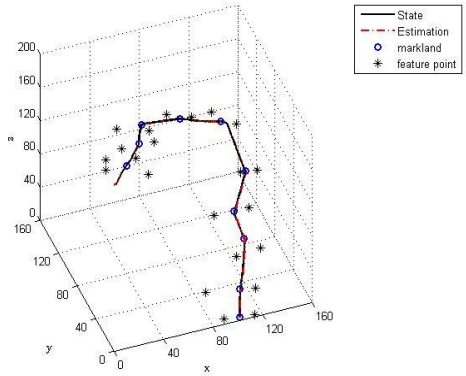

Figure 2. True trajectory of unmanned helicopter (black curve) and estimation of ERKF (red curve).

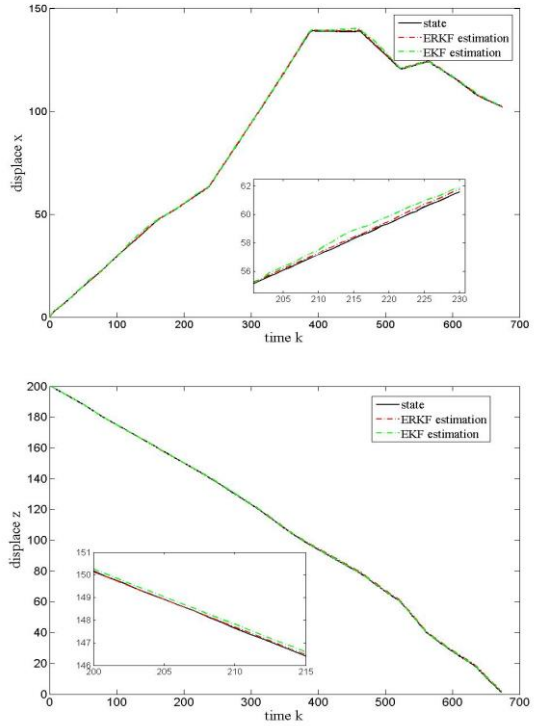

Figure 3. Trajectories x, z produced by different methods compared with true value respectively .

TABLE I. COMPARISON OF POSITION ESTIMATION ERRORS OF EKF AND ERKF.

	1	2	3	4	5	6	7	8	9	10	Mean
EKF	410.7	339.8	476.8	468.4	360.1	343.2	532.5	535.6	497.6	306.9	427.1
ERKF	397.8	298.9	300.5	288.3	194.1	338.1	280.9	292.1	205.6	255.0	**285.1**

B. Experiments on Datasets

Based on Section III, ERKF was integrated into the FAST-LIO2 and Point-LIO frameworks to evaluate its performance on open-source datasets, referred to as RS-FAST-LIO2 and RS-Point-LIO, respectively. Since ERKF cannot leverage the matrix inversion lemma to accelerate the computation of the innovation sequence covariance matrix, the time complexity of the filter is equivalent to that of standard EKF. To ensure the real-time performance of the system, an adaptive voxel size was employed for downsampling the point clouds. In this experiment, the number of point clouds per scan frame for both RS-FAST-LIO2 and RS-Point-LIO did not exceed 1200.

Drift Benchmark: We compared RS-FAST-LIO2, RS-Point-LIO, and their original versions using eleven sequences from the FAST-LIO2 [14] and R3LIVE [22] datasets, each ending at the starting position. Under the condition of consistent parameters for the corresponding frameworks, we calculated the end-to-end error, as shown in Table II. The ERKF is designed to enhance robustness in complex environments. As shown in the table, its accuracy is generally comparable to or slightly superior to that of the ISEKF algorithm. This suggests that by seeking suboptimal solutions, the ERKF algorithm effectively balances robustness and accuracy, performing well in both simple and complex environments without significantly compromising precision.

TABLE II. ABSOLUTE TRANSLATIONAL ERRORS (RMSE, METERS) IN SEQUENCES.

dataset	Sequence	FAST-LIO2	RS-FAST-LIO2	Point-LIO	RS-Point-LIO
Fastlio_1	100hz	0.350	0.209	0.339	**0.108**
Fastlio_2	Outdoor_Main	0.051	0.100	**0.014**	0.022
Fastlio_3	Outdoor_run	0.122	0.161	0.044	**0.033**
R3live_1	Campus_00	0.077	0.068	0.066	**0.006**
R3live_2	Campus_02	**0.019**	0.031	0.037	0.048
R3live_3	Campus_03	0.089	**0.039**	0.042	0.047
R3live_4	Hku_park_00	0.073	0.081	**0.018**	0.026
R3live_5	Hku_park_01	0.572	0.552	0.557	**0.490**
R3live_6	Hku_main_building	3.611	1.229	**0.061**	1.617
R3live_7	Deg_seq_00	6.080	5.700	5.531	**4.884**
R3live_8	Deg_seq_02	17.626	17.574	8.595	**7.440**
Average		3.160	2.793	1.436	**1.329**

C. *Real-world Experiments*

In real-world experiments, we control a magnetic adhesion wall-climbing robot (see Figure 4) to perform three-dimensional motion and eventually return to the starting position in two real-world environments, cabin and pipeline. We compare the performance of the FAST-LIO, RS-FAST-LIO, Point-LIO, and RS-Point-LIO algorithms using the RMSE of the start and end positions, as shown in Table III. In the cabin environment, the RMSE of FAST-LIO is 0.0986, while the RMSE of RS-FAST-LIO is 0.0951, a decrease in error of 3.55%. The RMSE of Point-LIO is 0.0908, while the RMSE of RS-Point-LIO is 0.0720, a decrease in error of 20.78%. In the pipeline environment, the RMSE of FAST-LIO is 0.0945, and the RMSE of RS-FAST-LIO is reduced to 0.0889, a decrease in error of 5.93%. The RMSE of Point-LIO is 0.1645, while the RMSE of RS-Point-LIO is reduced to 0.1349, a reduction of 17.99%. This demonstrates that incorporating the RS mechanism in the FAST-LIO framework can effectively reduce errors and improve positioning accuracy. In the Point-LIO framework, the improvement in error is more significant, especially in the cabin environment, where the error decrease exceeds 20%. Figure 5 show the two experimental scenes and the mapping results of RS-FAST-LIO.

Figure 5. The sensor uses the Livox MID-360 and is carried by a magnetic adhesion wall-climbing robot.

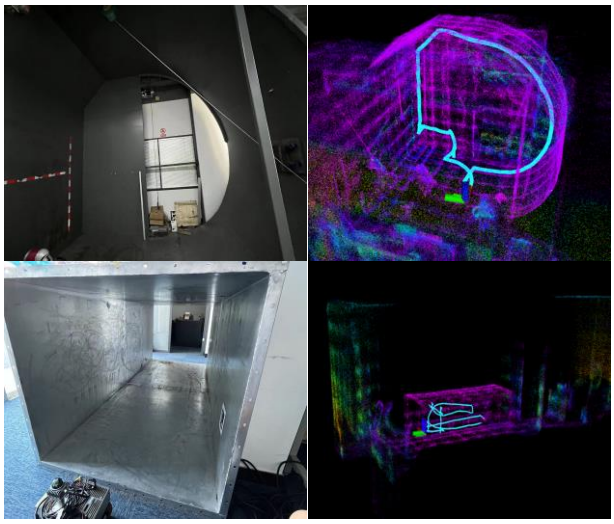

Figure 4. Cabin (up) and pipeline (down) test environments (left) and mapping results of RS-FAST-LIO (right).

TABLE III. ABSOLUTE TRANSLATIONAL ERRORS (RMSE, METERS) IN REAL-WORLD EXPERIMENTS.

Approach	Sequence	FAST-LIO	RS-FAST-LIO (θ=-.008)	Point-LIO	RS-point-LIO (θ=-.008)
Our_date1	Cabin	0.0986	**0.0951**	0.0908	**0.0720**
Our_date2	Pipeline	0.0945	**0.0889**	0.1645	**0.1349**

V. CONCLUSIONS

Extensive experiments on both benchmark and private datasets show that the ERKF-based backend SLAM framework can effectively enhance robustness in complex environments. It enables reliable state estimation even in the presence of uncertainty in noise parameters. In the future, we will focus on integrating fault diagnosis mechanisms and adaptive risk-sensitive coefficients to further improve the system's adaptability in dynamic and noise uncertainty environments.

ACKNOWLEDGMENT

The authors appreciate the FAST-LIO and Point-LIO teams for open-sourcing their excellent code and SLAM solutions.

The real-world experimental environment and the magnetic wall-climbing robot in this study were provided by Shanghai Juanji Special Equipment Co., Ltd. We sincerely acknowledge their support.

APPENDIX

A. *The proof of ERKF*

Review the derivation of the EKF in Section II, we can linearize the nonlinear systems (11), (12) in Krein-space as

$$\boldsymbol{x}_{k+1} = F_k \boldsymbol{x}_k + \widetilde{\boldsymbol{u}}_{k,1} + \boldsymbol{w}_k. \tag{18}$$

$$\begin{bmatrix} \boldsymbol{y_k} \\ \check{z}_{k|l} \end{bmatrix} = \begin{bmatrix} H_k \boldsymbol{x_k} + \widetilde{\boldsymbol{u}}_{\boldsymbol{k,2}} \\ L_k \boldsymbol{x_k} \end{bmatrix} + v_k. \tag{19}$$

For $\theta > 0$, a solution always exists since $\begin{bmatrix} R & 0 \\ 0 & \theta^{-1} I \end{bmatrix} > 0$ and the state-space model reduces to the usual Hilbert-space setting, and we're not going to talk about that.

For $\theta < 0$, we first need to prove the existence of the minimum value of $\tilde{J}_k$. Once the existence is established, select $\check{z}_{k|k}$ such that the minimum value of $\bar{J}_k$is positive definite. By deriving $\sum_{i=0}^{k} \varepsilon_i^{\mathrm{T}} R^{-1} \varepsilon_i$ in (10), we can obtain (20), where

$$\begin{bmatrix} y_k - h(\hat{x}_k^-) \\ \check{z}_{k|k} - \hat{z}_{k|k} \end{bmatrix} \triangleq$$

$$\begin{bmatrix} I & \\ -L_k P_k H_k^{\mathrm{T}} \left(R + H_k P_k H_k^{\mathrm{T}}\right)^{-1} & I \end{bmatrix} \begin{bmatrix} y_k - h(\hat{x}_k^-) \\ \check{z}_{k|k} - \hat{z}_{k|k-1} \end{bmatrix}. \tag{21}$$

Lemma 2 (The matrix inversion lemma). *Assume that C is nonsingular, then*

$$(A + BCD)^{-1} = A^{-1} - A^{-1} B (C^{-1} + DA^{-1}B)^{-1} DA^{-1}. \tag{22}$$

Using the Lemma 2, we may rewrite the (20) as (23).

Remark 2. *$\hat{z}_{k|k-1}$ is given by the Krein-space projection of $\check{z}_{k|k}$ onto the linear space $\mathcal{L}\left\{\{\boldsymbol{y}_i\}_{i=0}^{k-1}, \{\check{z}_{i|i}\}_{i=0}^{k-1}\right\}$, therefore, $\hat{z}_{k|k-1}$ is a linear function of $\{\boldsymbol{y}_i\}_{i=0}^{k-1}$. Further, $\hat{z}_{k|k}$ is given by the Krein-space projection of $\check{z}_{k|k}$ onto $\mathcal{L}\left\{\{\boldsymbol{y}_i\}_{i=0}^{k}, \{\check{z}_{i|i}\}_{i=0}^{k-1}\right\}$, thus $\hat{z}_{k|k}$ is a linear function of $\{\boldsymbol{y}_i\}_{i=0}^{k}$.*

Lemma 3. *If $\mathcal{P}_0 > 0$ and $Q > 0$, then the quadratic form J_k at the stationary point is*

$$J_k = \begin{bmatrix} \boldsymbol{y}_k \\ \check{z}_{k|k} \end{bmatrix}^{\mathrm{T}} R_{y,k}^{-1} \begin{bmatrix} \boldsymbol{y}_k \\ \check{z}_{k|k} \end{bmatrix},$$

the necessary and sufficient condition for this stationary point to be a minimum is that $R_{y,k}$ and $\begin{bmatrix} R & 0 \\ 0 & \theta^{-1} I \end{bmatrix}$ have the same inertia, where

$$R_{y,k} = \left\langle \begin{bmatrix} \boldsymbol{y_k} \\ \check{z}_{k|k} \end{bmatrix}, \begin{bmatrix} \boldsymbol{y_k} \\ \check{z}_{k|k} \end{bmatrix} \right\rangle.$$

Lemma 4. *The Gramian $R_{y,k}$ of y_k has the same inertia as the Gramian of the innovations $R_{e,k}$. The strong regularity of $R_{y,k}$ ensures the nonsingularity of $R_{e,k}$. Assume $R_{y,k} > 0$, iff*

$$R_{e,k} > 0.$$

From Lemma 3 and 4, a risk-sensitive estimator exists iff $\begin{bmatrix} R & 0 \\ 0 & \theta^{-1} I \end{bmatrix}$ and $R_{e,k}$ must have the same inertia. We can easily find that

$$R + H_k P_k H_k^{\mathrm{T}} > 0$$

and

$$\theta^{-1} I + L_k (P_k^{-1} + H_k^{\mathrm{T}} H_k)^{-1} L_k^{\mathrm{T}} < 0.$$

Further, since the stable point $\tilde{J}_k$ is positive, we must ensure that

$$\sum_{i=0}^{k} [y_k - h(\hat{x}_k^-)]^{\mathrm{T}} \left(R + H_k P_k H_k^{\mathrm{T}}\right)^{-1} [y_k - h(\hat{x}_k^-)]$$

$$+ \sum_{i=0}^{k} \left[\check{z}_{k|k} - \hat{z}_{k|k}\right]^{\mathrm{T}} \left[\theta^{-1} I + L_k \left(P_k^{-1} + H_k^{\mathrm{T}} H_k\right)^{-1} L_k^{\mathrm{T}}\right]^{-1}$$

$$\cdot \left[\check{z}_{k|k} - \hat{z}_{k|k}\right] > 0. \tag{24}$$

Obviously, we can choose that

$$\check{z}_{k|k} = \hat{z}_{k|k} = L_k \hat{x}_k^+,$$

where $\hat{x}_k^+$ is given by the Krein-space projection of $\boldsymbol{x}_k$ onto $\mathcal{L}\left\{\{\boldsymbol{y}_i\}_{i=0}^{k}, \{\check{z}_{i|i}\}_{i=0}^{k-1}\right\}$. Now we can perform Kerin-space KF recursive calculation on the state-space model (18) and (19) to solve for $\hat{x}_{k+1}^+$ as follows:

$$\hat{x}_{k+1}^+ = \hat{x}_{k+1}^- + P_{k+1} [H_{k+1}^{\mathrm{T}} \quad L_{k+1}^{\mathrm{T}}] R_{e,k+1}^{-1} \boldsymbol{\varepsilon}_{k+1}. \tag{25}$$

$$\tilde{J}_k = \sum_{i=0}^{k} \varepsilon_i^{\mathrm{T}} R_{e,k}^{-1} \varepsilon_i$$

$$= \sum_{i=0}^{k} \begin{bmatrix} y_k - h(\hat{x}_k^-) \\ \check{z}_{k|k} - \hat{z}_{k|k-1} \end{bmatrix}^{\mathrm{T}} \begin{bmatrix} R + H_k P_k H_k^{\mathrm{T}} & H_k P_k L_k^{\mathrm{T}} \\ L_k P_k H_k^{\mathrm{T}} & \theta^{-1} I + L_k P_k L_k^{\mathrm{T}} \end{bmatrix}^{-1} \begin{bmatrix} y_k - h(\hat{x}_k^-) \\ \check{z}_{k|k} - \hat{z}_{k|k-1} \end{bmatrix}$$

$$= \sum_{i=0}^{k} \begin{bmatrix} y_k - h(\hat{x}_k^-) \\ \check{z}_{k|k} - \hat{z}_{k|k} \end{bmatrix}^{\mathrm{T}} \begin{bmatrix} R + H_k P_k H_k^{\mathrm{T}} & \\ & \theta^{-1} I + L_k \left(P_k - P_k H_k^{\mathrm{T}} \left(R + H_k P_k H_k^{\mathrm{T}}\right)^{-1} H_k P_k\right) L_k^{\mathrm{T}} \end{bmatrix}^{-1} \begin{bmatrix} y_k - h(\hat{x}_k^-) \\ \check{z}_{k|k} - \hat{z}_{k|k} \end{bmatrix}. \tag{20}$$

$$\sum_{i=0}^{k} \begin{bmatrix} y_k - h(\hat{x}_k^-) \\ \check{z}_{k|k} - \hat{z}_{k|k} \end{bmatrix}^{\mathrm{T}} \begin{bmatrix} R + H_k P_k H_k^{\mathrm{T}} & \\ & \theta^{-1} I + L_k (P_k^{-1} + H_k^{\mathrm{T}} H_k)^{-1} L_k^{\mathrm{T}} \end{bmatrix}^{-1} \begin{bmatrix} y_k - h(\hat{x}_k^-) \\ \check{z}_{k|k} - \hat{z}_{k|k} \end{bmatrix}. \tag{23}$$

Choosing $\check{z}_{k+1|k+1} = \hat{z}_{k+1|k+1}$ and from the matrix inversion lemma, we can rewrite the above as follows

$$\hat{x}_{k+1}^{+} = \hat{x}_{k+1}^{-} + P_{k+1}H_{k+1}^{T}(R + H_{k+1}P_{k+1}H_{k+1}^{T})^{-1} \cdot [y_{k+1} - h(\hat{x}_{k+1}^{-})]. \quad (26)$$

REFERENCES

[1] T. Cui, C. Guo, Y. Liu and Z. Tian, "Precise Landing Control of UAV Based on Binocular Visual SLAM," *2021 4th International Conference on Intelligent Autonomous Systems*, 2021, pp. 312-317.

[2] Q. Zou, Q. Sun, L. Chen, B. Nie and Q. Li, "A Comparative Analysis of LiDAR SLAM-Based Indoor Navigation for Autonomous Vehicles," *IEEE Transactions on Intelligent Transportation Systems*, vol. 23, no. 7, pp. 6907-6921, July 2022.

[3] W. Wang, Y. Wu, Z. Jiang and J. Qi, "A Clutter-Resistant SLAM Algorithm for Autonomous Guided Vehicles in Dynamic Industrial Environment," *IEEE Access*, vol. 8, pp. 109770-109782, 2020.

[4] J. Oršulić, R. Milijas, A. Batinovic, L. Markovic, A. Ivanovic and S. Bogdan, "Flying with Cartographer: Adapting the Cartographer 3D Graph SLAM Stack for UAV Navigation," *2021 Aerial Robotic Systems Physically Interacting with the Environment (AIRPHARO)*, 2021, pp. 1-7.

[5] Y. Luo, Y. Li, Z. Li and F. Shuang, "MS-SLAM: Motion State Decision of Keyframes for UAV-Based Vision Localization," *IEEE Access*, vol. 9, pp. 67667-67679, 2021.

[6] J. Covolan, A. Sementille and S. Sanches, "A mapping of visual SLAM algorithms and their applications in augmented reality," *2020 22nd Symposium on Virtual and Augmented Reality*, 2020, pp. 20-29.

[7] J. Yin, A. Li, W. Xi, W. Yu and D. Zou, "Ground-Fusion: A Low-cost Ground SLAM System Robust to Corner Cases," *2024 IEEE International Conference on Robotics and Automation (ICRA)*, Yokohama, Japan, 2024, pp. 8603-8609.

[8] Y. Wang, Y. Ng, I. Sa, A. Parra, C. Rodriguez-Opazo, T. Lin and H. Li, "MAVIS: Multi-Camera Augmented Visual-Inertial SLAM using SE2(3) Based Exact IMU Pre-integration," *2024 IEEE International Conference on Robotics and Automation (ICRA)*, 2024, pp. 1694-1700.

[9] T. Shan, B. Englot, D. Meyers, W. Wang, C. Ratti, and D. Rus, "Lio-sam: Tightly-coupled lidar inertial odometry via smoothing and mapping," in *2020 IEEE/RSJ International Conference on Intelligent Robots and Systems (IROS)*, 2020, pp. 5135–5142.

[10] M. Li and A. Mourikis, "High-precision, consistent ekf-based visual-inertial odometry," *International Journal of Robotics Research*, vol. 32, pp. 690-711, MAY 2013.

[11] Y. Zhang, T. Zhang and S. Huang, "Comparison of EKF based SLAM and optimization based SLAM algorithms," *2018 13th IEEE Conference on Industrial Electronics and Applications (ICIEA)*, 2018, pp. 1308-1313.

[12] A. Barrau and S. Bonnalel, "The Invariant Extended Kalman filter as a stable observer," *IEEE Transactions on Automatic Control*, vol. 62, no. 4, pp. 1797-1812.

[13] P. Wu, Z. Shi and P. Yan, "Improved EKF-SLAM Algorithm of Unmanned Helicopter Autonomous Landing on Ship," *2018 37th Chinese Control Conference (CCC)*, 2018, pp. 5287-5292.

[14] W. Xu, Y. Cai, D. He, J. Lin and F. Zhang, "FAST-LIO2: Fast Direct LiDAR-Inertial Odometry," in *IEEE Transactions on Robotics*, vol. 38, no. 4, pp. 2053-2073, Aug. 2022.

[15] D. He, W. Xu, N. Chen, F. Kong, C. Yuan and F. Zhang, "Point-LIO: Robust High-Bandwidth Light Detection and Ranging Inertial Odometry." *Adv. Intell. Syst*., 5: 2200459, 2023.

[16] C. Zheng et al., "FAST-LIVO2: Fast, Direct LiDAR–Inertial–Visual Odometry," in *IEEE Transactions on Robotics*, vol. 41, pp. 326-346, 2025.

[17] B. Hassibi, A. Sayed and T. Kailath, "Linear estimation in Krein spaces. I. Theory," *IEEE Transactions on Automatic Control*, vol. 41, no. 1, pp. 18-33, Jan. 1996.

[18] B. Hassibi, A. Sayed and T. Kailath, "Linear estimation in Krein spaces. II. Applications," *IEEE Transactions on Automatic Control*, vol. 41, no. 1, pp. 34-49, Jan. 1996.

[19] A. Jordana, A. Meduri, E. Arlaud, J. Carpentier and L. Righetti, "Risk-Sensitive Extended Kalman Filter," *2024 IEEE International Conference on Robotics and Automation (ICRA)*, 2024, pp. 10450-10456.

[20] Y. Luo, Q. Su, Y. Zhang, X. Zheng, "Improved Rao-Blackwellized H_∞ filter based mobile robot SLAM," *The Journal of China Universities of Posts and Telecommunications*, vol. 23, no. 5, pp. 47-55, 2016.

[21] P. Geneva, K. Eckenhoff, W. Lee, Y. Yang and G. Huang, "OpenVINS: A Research Platform for Visual-Inertial Estimation," *2020 IEEE International Conference on Robotics and Automation (ICRA)*, Paris, France, 2020, pp. 4666-4672,

[22] J. Lin and F. Zhang, "R3LIVE: A Robust, Real-time, RGB-colored, LiDAR-Inertial-Visual tightly-coupled state Estimation and mapping package," *2022 International Conference on Robotics and Automation (ICRA)*, Philadelphia, PA, USA, 2022, pp. 10672-10678,